

Algebraic quantification of an active region's contribution to the solar cycle

Zi-Fan Wang^{1,2}, Jie Jiang^{3,4}, and Jing-Xiu Wang^{2,1}

¹ Key Laboratory of Solar Activity, National Astronomical Observatories, Chinese Academy of Sciences, Beijing 100101, China

² School of Astronomy and Space Science, University of Chinese Academy of Sciences, Beijing, China

³ School of Space and Environment, Beihang University, Beijing, China

⁴ Key Laboratory of Space Environment Monitoring and Information Processing of MIIT, Beijing, China

December 26, 2021

ABSTRACT

Context. The solar dipole moment at cycle minimum is considered to be the most successful precursor for the amplitude of the subsequent cycle. Numerical simulations of the surface flux transport (SFT) model are widely used to effectively predict the dipole moment at cycle minimum. Recently an algebraic method has been proposed to quickly predict the contribution of an active region (AR) to the axial dipole moment at cycle minimum instead of SFT simulations. However, the method assumes a bipolar magnetic region (BMR) configuration of ARs. Actually most ARs are asymmetric in configuration of opposite polarities, or have more complex configurations. Such ARs evolve significantly differently from that of BMR approximations.

Aims. We propose a generalized algebraic method to describe the axial dipole contribution of an AR with an arbitrary configuration, and evaluate its effectiveness compared to the BMR-based method.

Methods. We employ mathematical deductions to obtain the generalized method. We compare the results of the generalized method with SFT simulations of observed ARs, artificially created BMRs, and ARs with more complex configurations. We also compare the results with that from the BMR-based method.

Results. The generalized method is equivalent to the SFT model, and precisely predicts the ARs' contributions to the dipole moment. The method has a much higher computational efficiency than SFT simulations. Although the BMR-based method has similar computational efficiency as the generalized method, it is only accurate for symmetric bipolar ARs. The BMR-based method systematically overestimates the dipole contributions of asymmetric bipolar ARs, and randomly miscalculate the contributions of more complex ARs.

Conclusions. The generalized method provides a quick and precise quantification of an AR's contribution to the solar cycle evolution, which paves the way for the application into the physics-based solar cycle prediction.

Key words. Sun: activity – sunspots – Sun: magnetic fields

1. Introduction

The sun's long-term magnetic activity variations are the major source of influence to space climate, affecting the solar wind, the heliosphere, and the related planetary environments (Mursula et al. 2007; Nandy & Martens 2007). The long-term development of the solar magnetic field is described by the solar dynamo mechanism, of which the elementary mode is the 22-year magnetic cycle. As described by the Babcock-Leighton dynamo (Babcock 1961; Leighton 1964, 1969), the initial poloidal field at cycle minimum, mostly composed of the polar field, is the source of the toroidal field responsible for the solar active regions during solar cycle (Jiang et al. 2013; Cameron & Schüssler 2015). Hence, the polar field at the cycle minimum is often regarded as the precursor of the next cycle's strength (Schatten et al. 1978; Wang 2017; Jiang et al. 2018; Petrovay 2020). As the polar field is subject to different definitions, the axial dipole moment of the surface magnetic field is often studied as an equivalent. The dipole moment is introduced by active regions (ARs) that bear initial dipole moments as a result of Joy's law (Hale et al. 1919). An AR's dipole moment evolves as the surface flux transport (SFT) process takes place, and contributes to the dipole moment at cycle minimum, hereafter referred to as the final dipole moment. Therefore, the contribution of an AR to the final dipole moment quantifies its influence on the long-term development of the solar cycle, as described by the dipole index introduced by Jiang et al. (2019), and by the index ARDoR, i.e., Active Region Degree of Rogueness introduced by Nagy et al. (2020).

The contribution of an AR to the solar cycle is commonly obtained by numerical simulations based on the SFT model (e.g. DeVore et al. 1985; Wang et al. 1989; van Ballegoijen et al. 1998; Mackay et al. 2002; Jiang et al. 2014). Meanwhile, it can also be deduced from an algebraic form dependent on the properties of the AR directly, while actual simulations are

not necessary. As shown by the SFT simulations of Jiang et al. (2014), and by the mathematical deductions of Petrovay et al. (2020), the initial dipole introduced by an AR, D_i , and its contribution to the final dipole, D_f , follow Eq. (1)

$$\frac{D_f}{D_i} = A \exp\left(\frac{-\lambda^2}{2\lambda_R^2}\right), \quad (1)$$

where λ is the emerging latitude of the AR, A and λ_R are constants related to the transport processes.

Eq. (1) assumes that the ARs emerge in the form of bipolar magnetic regions (BMRs). Hereafter we refer to Eq. (1) as the BMR-based method. The BMR approximation is unrealistic for ARs. The two polarities of an AR may be asymmetrical in size and flux, affecting its surface evolutions and contribution to the final dipole (Iijima et al. 2019). An AR with more complex configurations, e.g. a δ -type AR, may deviate from or even be opposite to the predictions of the BMR-based method (Jiang et al. 2019). Generally, ARs with real configurations produce notably different dipole evolutions from that produced by their corresponding BMR approximations (Yeates 2020). Hence, it is not precise to include the BMR approximation when quantifying the ARs' contributions to the solar cycle, and ARs' configurations should be considered. The current function form of the BMR-based method cannot include ARs' configurations directly. The Gaussian function in Eq. (1) assigns the whole AR with a certain latitude. However, as we decompose a realistic AR into smaller bipolar components, the latitudes of these regions are different. Hence, an algebraic method that includes ARs' configurations by considering ARs' smaller components is required. Since the SFT model is linear when nonlinear feedbacks of magnetic fields on the velocity profiles (e.g. inflows toward activity belts, see Gizon 2004; Jiang et al. 2010; Cameron & Schüssler 2010; Nagy et al. 2020) are not considered, the function describing such elementary components contributing to the final dipole should be linearly addable, so that we can divide an complex AR into its elementary components, and evaluate the contributions of these elementary components separately, and sum them up. Hence, such an algebraic method will be capable of predicting the final dipole contribution of an arbitrary AR, and produce a valid quantification of its contribution to the solar cycle without SFT numerical simulations.

We propose a generalized algebraic method to predict the final dipole contribution of ARs with arbitrary magnetic configurations, by generalizing the analytic approach of Petrovay et al. (2020). We use SFT simulations of ARs to assess the accuracy of the final dipole contribution predictions of the new generalized method, and the predictions of the previous BMR-based method. We will demonstrate that the generalized method is a theoretical approximation and quick implement of the SFT simulations, while the previous BMR-based method is only its special case. As ARs' configurations are considered, the new generalized method produces better predictions of final dipole than previous methods, and soundly quantifies the contributions of arbitrary ARs to the solar cycle evolution.

The article is organized as follows. In Sect. 2 we describe the mathematical foundations and deduction of the generalized algebraic method. In Sect. 3 we introduce the SFT simulation model which is applied to evaluate the algebraic methods. In Sect. 4 we evaluate the algebraic methods with the results of SFT simulations. We discuss and conclude in Sect. 5.

2. Deduction of the algebraic method to predict dipole contribution of ARs

The basic equation of the SFT model is the radial component of the magnetic induction equation at the solar surface, as shown by Eq. (2), where $B(\theta, \phi, t)$ is the surface radial field at a certain colatitude θ , longitude ϕ , and time t . $\Omega(\theta)$ denotes the differential rotation, $v(\theta)$ denotes the meridional flow, and η denotes the supergranular diffusion. New flux emergence is inserted as $S(\theta, \phi, t)$. As the velocity profiles are usually predetermined and independent of B , the equation is linear in terms of B , thus allowing the superposition of contributions of different magnetic flux sources.

$$\begin{aligned} \frac{\partial B}{\partial t} = & -\Omega(\theta) \frac{\partial B}{\partial \phi} - \frac{1}{R_\odot \sin \theta} \frac{\partial}{\partial \theta} [v(\theta) B \sin(\theta)] + \\ & \frac{\eta}{R_\odot^2} \left[\frac{1}{\sin \theta} \frac{\partial}{\partial \theta} \left(\sin \theta \frac{\partial B}{\partial \theta} \right) + \frac{1}{\sin^2 \theta} \frac{\partial^2 B}{\partial \phi^2} \right] + \\ & S(\theta, \phi, t) \end{aligned} \quad (2)$$

As an emerged AR evolves according to the SFT processes, the generated cross-equatorial flux is important for the large-scale surface field and the final dipole moment (Cameron et al. 2013; Wang 2017). The cross-equatorial flux is a result of the competition between diffusion and meridional flow, and leads to total flux difference in the two hemispheres. The flux difference determines the final dipole moment. The analytic approach of deducing the BMR-based algebraic method by Petrovay et al. (2020) follows this concept. They discussed the cross-equatorial flux ratio generated by a unipolar flux patch with a Gaussian profile

$$B(\lambda) = \frac{a}{\sigma_0} \exp\left[-\frac{(\lambda - \lambda_0)^2}{2\sigma_0^2}\right], \quad (3)$$

at a certain latitude λ_0 with a certain width σ_0 . Assuming a near equator Cartesian approximation where the 1st order Taylor expansion of the meridional flow was considered, they proved that the fraction of cross-equatorial flux of the

Gaussian flux patch on the northern hemisphere is as follows:

$$f_{crossed} = \frac{1}{2} \left[1 - \operatorname{erf} \left(\lambda_0 / \sqrt{2} \lambda_R \right) \right]. \quad (4)$$

The parameter λ_R is

$$\lambda_R = \sqrt{\sigma_0^2 + \frac{\eta}{R^2 \Delta_u}}, \quad (5)$$

where R is the solar radius, and Δ_u is the derivative of the meridional flow at the equator. Hence, the cross-equatorial flux is dependent on the initial configuration as well as the transport terms. They then assumed two flux patches of different polarities, that is, BMRs, and proved Eq. (1).

We consider an arbitrary flux region, rather than the BMR form. Because the SFT model shown by Eq. (2) is linear, the contribution of an arbitrary AR to the final dipole moment is a linear addition of the contribution of its smaller parts. Considering the limit, an arbitrary AR can be decomposed into infinite sizeless ‘‘points’’. Such points are unipolar regions corresponding to magnetogram pixels in reality. In fact, we know,

$$\lim_{\sigma_0 \rightarrow 0} \left\{ \frac{a}{\sigma_0} \exp \left[-\frac{(\lambda - \lambda_0)^2}{2\sigma_0^2} \right] \right\} = a\sqrt{2\pi}\delta(\lambda - \lambda_0), \quad (6)$$

where $\delta(\lambda - \lambda_0)$ is the Dirac δ function, and a is a constant. From this perspective, Eqs. (4) and (5) also hold for such a ‘‘point’’. The difference is that λ_R in this case is dependent on transport terms only.

The flux difference in the two hemispheres generated by the point can be deduced from the cross-equatorial flux. Assuming that at cycle minimum the polar field follows a certain profile determined by the balance of diffusion and meridional flow, the final dipole moment generated by the point $D_{f,point}$ is proportional to the flux difference in the two hemispheres,

$$D_{f,point} \propto \operatorname{erf} \left(|\lambda_0| / \sqrt{2} \lambda_R \right) \operatorname{sgn}(\lambda_0) \quad (7)$$

Here we add a sign function $\operatorname{sgn}(\lambda_0)$ to put different hemispheres into consideration.

The contribution of the whole AR to the final dipole is an integration over the AR,

$$D_f = A_0 \iint B(\theta, \phi) \operatorname{erf} \left(|\lambda_0| / \sqrt{2} \lambda_R \right) \operatorname{sgn}(\lambda_0) \sin \theta d\theta d\phi \quad (8)$$

This is the generalized algebraic method we introduce. Any arbitrary AR can be calculated by integrating over it, and the parameter λ_R , which now equals $\sqrt{\frac{\eta}{R^2 \Delta_u}}$, is independent on AR configuration. In practice, the numerical integration is carried out by the trapezoidal rule in this article. In this way, D_f is calculated by summing the final dipole contributions of all pixels of the AR.

The proportion ratio A_0 originates from the proportional relationship between the axial dipole moment and flux difference in the two hemispheres. As mentioned above, A_0 is determined by the balance of diffusion and meridional flow, so it is dependent on the strength of diffusion and the meridional flow profile. Hence, A_0 varies with SFT models with different transport parameters, but the proportional relationship is not affected by the exact transport parameters. A_0 is a scaling factor when the parameters of the SFT model are given. We will obtain A_0 by considering the simulations of the SFT model, fitting A_0 from the results of algebraic methods and SFT simulations.

The generalized algebraic method significantly fastens the acquisition of final dipole contributions for ARs, compared to SFT simulations, as actual numerical calculations are no longer required. Compared to the BMR-based method (Petrovay et al. 2020), the generalized algebraic method costs the same orders of computation time, considering the calculation methods. The generalized method described by Eq. (8) is an integration over the evaluated AR. Meanwhile, the BMR-based method requires the initial dipole moment D_i of the AR, so integrating over the AR is also required. The integration is,

$$D_i = \frac{3}{4\pi} \iint B(\theta, \phi) \cos \theta \sin \theta d\theta d\phi. \quad (9)$$

Hence, if the generalized method and the BMR-based method adopt the same numerical integration algorithm, and are applied to the same magnetogram, the computation time will be similar.

3. Simulations based on the SFT model

To justify the generalized method, and to compare its effectiveness with the previous BMR-based method, we run SFT simulations for some ARs, and compare the results between the simulations and the prediction methods. We use an SFT code to solve Eq. (2) based on Baumann et al. (2004). The spatial resolution of the code is 360×180 , and its time interval is 1 day. The spatial part is decomposed into spherical harmonics up to order 63, and the temporal part is solved with the 4th order Runge-Kutta method.

The differential rotation profile is adopted from Snodgrass (1983). The meridional flow profile is adopted from van Ballegoijen et al. (1998) with the flow speed set as 11 ms^{-1} . The supergranular diffusion is $500 \text{ km}^2\text{s}^{-1}$. Under this set of transport parameters, λ_R for the generalized method is equal to $9^\circ.45$. We use this value in the following evaluations of the generalized method.

Each AR is simulated for 10 years separately to reach the final state to get the final dipole contribution. To compare with the results of the BMR-based method, each AR is related to its latitude, represented by the average latitude weighted by unsigned flux. We use two kinds of ARs in the simulations: the ARs from observations of a continuous time period, and the ARs artificially created from predetermined parameters.

For observational ARs, we choose ARs during Carrington Rotations (CRs) 2145-2159, as these ARs are recognized as important in the cycle development of cycle 24, and contribute a large fraction to the final dipole, shown by the SFT simulations of Wang et al. (2020). Here we adopt the 84 ARs identified and used in their work, in which the characteristics and evolution properties are discussed in detail. Some of these ARs bear complex configurations instead of simple BMR form, as presented by Wang et al. (2020).

For artificially created ARs, we consider bipolar ARs and ARs with complex configurations. The bipolar ARs are composed of two Gaussian flux patches of opposite polarities (Baumann et al. 2004; Jiang et al. 2014). The maximum magnetic field strength is set to 250 G, and the tilt angles of the bipolar ARs are determined by Joy's law, $\alpha = k\sqrt{|\lambda|}$, where α is the tilt angle and $k = 1.3$ is a typical value of the Joy's coefficient (Cameron et al. 2010; Jiang 2020). The latitudes considered range from 0° to 35° with a 5° interval, covering 8 latitudes in total. In this form, the bipolar ARs at 0° latitude have no tilts, so their initial dipoles are also 0. In order to show the influence of AR configurations to the prediction methods, we include morphological asymmetries of the two polarities, which were introduced by Iijima et al. (2019). With an asymmetry factor f_{asym} , the maximum field strengths B_{max} and the widths of the Gaussian profiles σ_0 are modified as,

$$f_{asym} = \frac{B_{max,L}}{B_{max,F}} = \left(\frac{\sigma_{0,F}}{\sigma_{0,L}} \right)^2 \quad (10)$$

where the subscript L indicates the leading polarity and the subscript F indicates the following polarity, identical to the factor defined by Iijima et al. (2019). In this way, the following polarity is more diffusive. We consider the cases where f_{asym} equals 1, 2, and 3, and refer to them as the symmetric, weakly asymmetric, and strongly asymmetric cases, respectively.

To compare with the results of bipolar ARs, we also create ARs with more complex configurations at certain latitudes. The ARs are modelled after NOAA AR 12673, which was studied in detail by Jiang et al. (2019). As shown by their work, AR 12673 is a typical case where the SFT model produces significantly different results from the BMR-based model as a result of its complex configuration. Here we flip it into the northern hemisphere to compare with the aforementioned artificially generated bipolar ARs, and shift its latitudinal locations of each pixel in the equal-latitude projection. The complex ARs' latitudes, defined as area weighted flux center, are now also from 0° to 35° with a 5° interval.

4. Evaluating the generalized algebraic method with SFT simulations

4.1. Evaluation using observed ARs

We compare the simulated final dipole moment for the observed ARs during CRs 2145-2159 with the results by the algebraic prediction methods. For the generalized algebraic method, we compute the integration for each isolated AR over the whole solar surface, with the constant λ_R given in Sect. 3. Since the SFT simulations decompose the surface magnetic field into spherical harmonics up to order 63, we also apply the integration over the ARs with their spherical harmonics components up to order 63, while the higher orders are not included in the integration, for the consistency of numerical methods. The value of the coefficient A_0 in Eq. (8) is 0.21, which is obtained by linear fitting the simulated dipole contributions to the results of Eq. (8).

The results of the simulated final dipole moment and corresponding final dipole moment predicted by the generalized method for each AR are displayed in Fig. 1(a). As shown, the predictions of the generalized algebraic method are almost identical to the results of SFT simulations. The maximum difference between the predicted and simulated final dipole is 0.009G (11% of the dipole contribution from the AR that generates the maximum difference), represented by the grey shade. As shown by the grey shade, the error of the final dipole is actually not directly related to the absolute value of the final dipole. The error may originate from the deviation from the near-equator Cartesian assumption and the lowest order Taylor approximation of the meridional flow when we deduce the algebraic method. The method is a practical and effective simplification of the SFT model, as expected by the mathematical arguments in Sect. 2.

We compare the results of the generalized algebraic method with the BMR-based method. To utilize the BMR-based method, we calculate the initial dipole moment D_i for each AR. Similarly, the integration is calculated based on the ARs

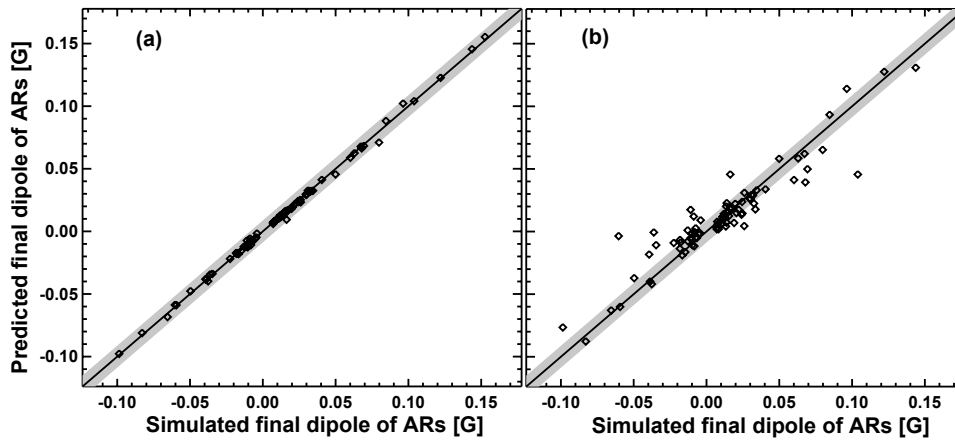


Fig. 1. Comparisons of the ARs' final dipoles between the SFT simulated one and the predictions by the algebraic methods. Each diamond represents an AR during CRs 2145-2159. The horizontal x axis represents the final dipole produced by SFT simulations. The vertical y axis represents the final dipole predicted by algebraic methods. Panel (a) presents the results of the generalized method that we introduce; panel (b) presents the results of the BMR-based method. The diagonal line represents $y = x$. The grey shade represents the region where the final dipole produced by the algebraic methods has no larger than 0.009G deviation from the result produced by SFT simulations.

with their spherical harmonics components up to order 63. The initial dipole moments are multiplied by corresponding contribution factor D_f/D_i . According to Eq. (5), λ_R depends on σ_0 , the initial Gaussian width of the polarities, which is not a well-defined quantity for ARs with real configurations. Hence, we adopt the value $\lambda_R = 10^\circ.06$ fitted from the symmetric bipolar ARs in Sect. 4.2, in which case λ_R makes sense strictly. The results by the BMR-based method are displayed in Fig. 1(b). The scatter of the points is considerably larger than the generalized method. The maximum difference between predictions and simulation is now 0.06G (56% of the dipole contribution of the AR), produced by NOAA AR 11990 on CR 2157. AR 11990 is located within the corresponding area of AR 11967, which is a complex $\beta\gamma\delta$ type AR on CR 2156. The remnant of AR 11967 causes the identified AR 11990 to be very asymmetric, resulting a large deviation. This shows that the BMR-based method is not accurate when the flux emergence is in more complex forms.

To further demonstrate the deviation of D_f/D_i with realistic ARs' configurations from the values with the BMR approximations, we plot D_f/D_i for each AR in Fig. 2. As shown, while there appears to be a Gaussian trend expressed by Eq. (1) and indicated by the red curve, many points deviate from the trend, similar to the results of Yeates (2020). Hence, the BMR-based method is limited for ARs in reality, while the generalized method produces more reliable predictions as ARs' configurations are considered. Please note that although Fig. 1(b) and Fig. 2 show that the BMR-based method tends to give lower predicted final dipole moments, this is not necessary the case. The trend results from limited ARs considered by us. For enough amount of ARs, there is no trend as shown by Fig. 8 of Yeates (2020). The BMR-based method could give a stronger or lower predicted final dipole moment depending on the configuration of the AR, which will be explained in Sect. 4.2.

4.2. Evaluation using artificially created ARs

In order to evaluate the generalized method, and to explicitly show the difference between the generalized method and the previous BMR-based method, we employ both methods to predict the four sets of artificially created ARs. A set of examples of the ARs is displayed in Fig. 3. As shown, the ARs with different degrees of asymmetries differ in their following polarities, while the complex AR is completely different from the bipolar ARs.

The artificially created ARs are simulated to get their corresponding final dipole contributions. We also calculate the results of the two algebraic prediction methods for the ARs as described in Sect. 4.1. The corresponding contribution factors D_f/D_i are plotted in Fig. 4. Since the bipolar ARs at the equator do not have initial dipole due to zero tilt angle, they are not shown here. As shown, the different cases do not follow a uniform trend. The bipolar ARs with different degrees of asymmetries (marked with black diamonds, purple triangles, and blue squares) appears in separate trends. The bipolar ARs with more diffusive following polarities are systematically overestimated by the BMR-based method, as they all appear under the trend line. This indicates that they produce less contributions to the final dipole moment as more flux of the following polarity tend to migrate across the equator, which agrees with the results of Iijima et al. (2019). For the strongly asymmetric cases, the contributions predicted by the BMR-method become even opposite to the SFT simulations at some latitudes. The results of the complex ARs based on the configuration of AR 12673 (marked with red asterisks) does not follow a trend at all, and the contribution factor even becomes negative for some cases, as Jiang et al. (2019) have introduced. In summary, for the asymmetric bipolar ARs illustrated by the artificially created ones, the BMR-based method systematically overestimates the dipole contribution, while for the complex ARs, the dipole contribution given by the BMR-based method does not show a systematic trend.

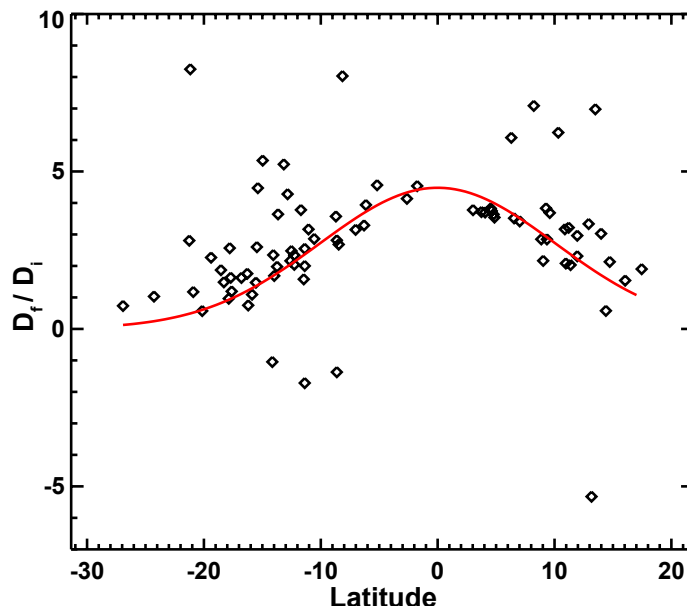


Fig. 2. Final dipole contribution factor D_f/D_i , with each diamond representing an AR during CRs 2145-2159. The red trend line, representing Eq. (1), is plotted by setting $\lambda_R = 10^\circ.06$.

The results of the artificially created ARs are consistent with the results of observed ARs in Sect. 4.1. From the perspective of Eq. (8), the major contribution of an AR to the final dipole originates from its components with lower latitudes and higher fluxes, instead of the properties of the whole AR. Hence, for ARs with irregularly distributed flux, the final dipole contributions deviate from the predictions of the BMR-based method, which considers the ARs' overall properties only. The deviation depends on the exact configuration of ARs instead of a systematic property. Even for ARs with the same shape, a slight change in latitude changes the contributions vastly, as shown by the red asterisks in Fig. (4). Since many observed ARs are not bipolar in reality, the BMR-based method tends to randomly miscalculate the results instead of a systematic deviation.

Now we deal with the 4 kinds of configurations of ARs located at different latitudes in the same way as Fig. 1. The results are shown in Fig. 5. Figure 5(a) indicates that the generalized algebraic method still produces reliable final dipole predictions for all cases. The different configurations of the ARs do not affect the results notably. On the contrary, the BMR-based method cannot produce reliable predictions for the asymmetric or complex cases (Fig. 5(b)). The asymmetric bipolar ARs (purple triangles and blue squares) deviate from the main trend of the symmetric BMRs, and the complex ARs (red asterisks) are completely irregularly distributed. As clarified above, this can be explained by the fact that, the parameter λ_R is not fixed when the initial configuration of the flux patches are not as diffusive as others, and is completely ill-defined for complex ARs. The generalized method, however, is free from the problem, as it does not involve BMR assumptions. The generalized method maintains its accuracy regardless of different AR configurations. We explicitly show that, the generalized method is a more generalized approximation of the SFT model, while the previous BMR-based method considers only a special case.

5. Discussion and conclusions

We have introduced a generalised algebraic method to calculate the contribution of an arbitrary AR to the axial dipole moment at cycle minimum, which is the precursor of the next cycle's strength. The method is a time-efficient alternative of the SFT simulations to predict the ARs' final dipole contributions. The method describes the cross-equatorial flux transport originating from a point magnetic flux patch, i.e. described by a Dirac δ function profile flux, and deduces the associated final dipole moment contribution. The contribution of an arbitrary AR to the final dipole moment is an integration of the points' contributions covering all the AR area. This method is a generalization of the previous Gaussian contribution profile method, which assumes the flux emergence in the form of BMRs with fixed width (Petrovay et al. 2020). We have explicitly shown that the generalized method is not affected by ARs' configurations as the BMR-based method is, by comparing to simulations of artificially created BMRs with different degrees of asymmetry and more complex ARs. The generalized method produces more accurate dipole predictions compared to the BMR-based method for realistic ARs, and costs considerably less computation time than SFT simulations. On the contrary, the BMR-based method tends to systematically overestimate the contributions of asymmetric bipolar ARs, and randomly miscalculate the contributions of ARs with complex configurations. Hence, the generalized method offers a quick alternative of SFT simulations to precisely quantify an AR's influence to the solar cycle evolution, thus improving the understanding of physics-based solar cycle predictions.

While the generalized algebraic method we introduce can precisely predict the ARs' contributions to the final dipole moment, the algebraic method does not produce the whole process of the development of the large-scale magnetic field,

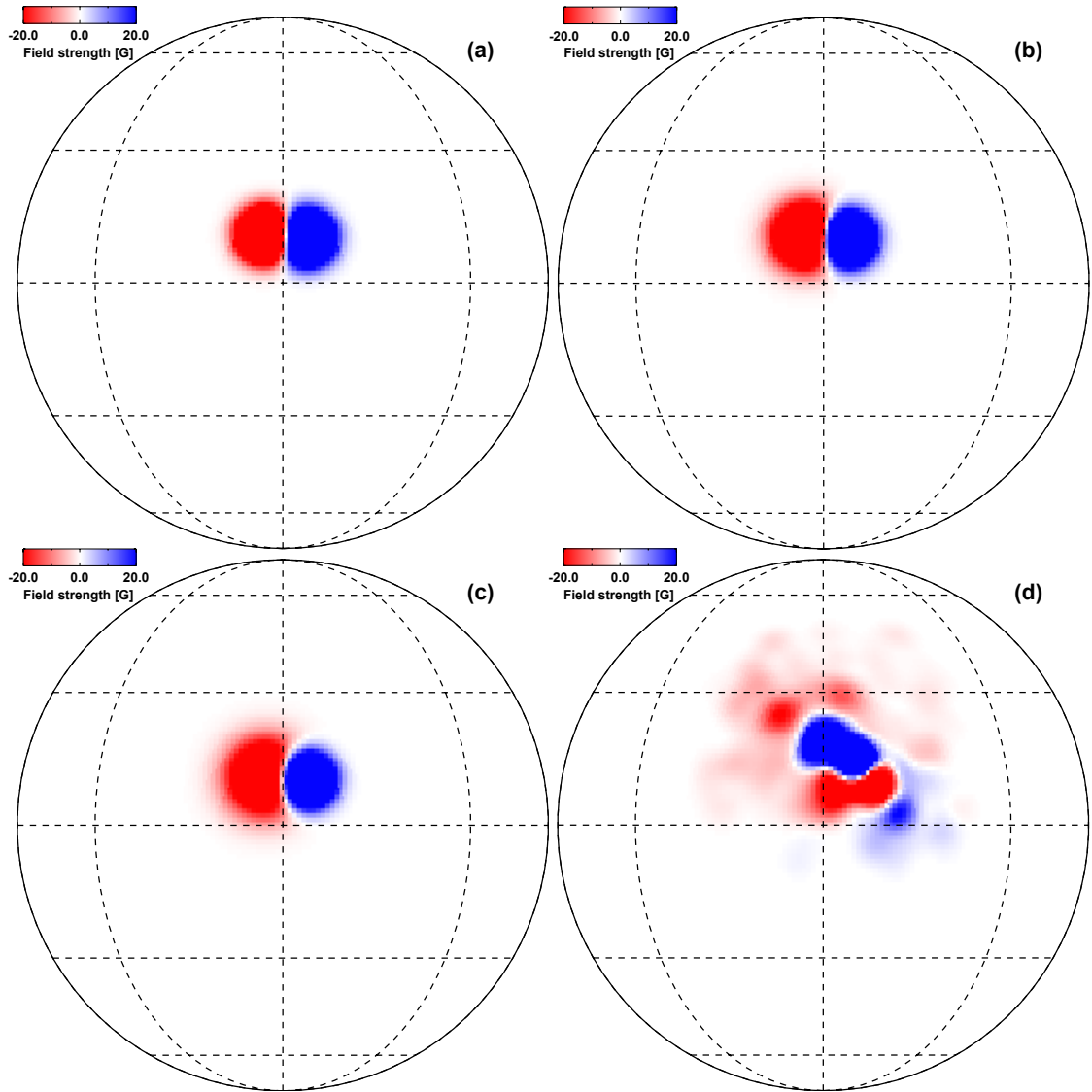


Fig. 3. Examples of the artificially created ARs with different types of configurations: (a) symmetric bipolar AR; (b) weakly asymmetric bipolar AR; (c) strongly asymmetric bipolar AR; (d) complex AR. The examples are orthographically projected.

so SFT simulations are still required to understand the development of solar magnetism at the solar surface and the heliosphere. The algebraic method does not replace the needs of realistic SFT simulations.

The generalized algebraic method is valid for any linear, kinematic SFT model regardless of transport parameters and profiles. An SFT model with different assumptions of the transport terms can also be described by the algebraic method, but the exact parameters of the method may be different. Therefore, the method is universal for SFT models, but the results of the method is limited to a specific SFT model with a set of given transport parameters. When we use the algebraic method to quantify ARs' contributions to the solar cycle in the future, the parameters λ_R and A_0 should be derived from the transport parameters of the specific SFT model we adopt.

The generalized algebraic method is a theoretical approximation and quick implement of the SFT model, while the previous BMR-based method is its special case. The SFT model describes the emerged ARs after reaching their decay phase, not the flux emergence of ARs. The generalized algebraic method cannot describe the emergence of ARs either. Therefore, the ARs should be accurately identified on their decay phase to precisely quantify their contributions to the solar cycle. For ARs that emerge in proximate to others spatially and temporally, automatically identifying its exact decay phase can be problematic, as the fluxes of different ARs often superpose with each other as they evolve (Wang et al. 2020). This problem should be considered as we analyze and characterize an AR's influence on the solar cycle.

The generalized method requires the real configurations of ARs, so the spatial resolution of the input ARs needs to be carefully considered. To what extent are the details of the ARs needed? Theoretically, the SFT model implements the supergranular diffusion, which is introduced by the random walk process from the supergranulation convective currents (Leighton 1964). This potentially limits the resolution of the SFT model and its algebraic equivalent method. Further numerical and observational studies are needed to clarify the required ARs' resolution, such as the previous efforts of

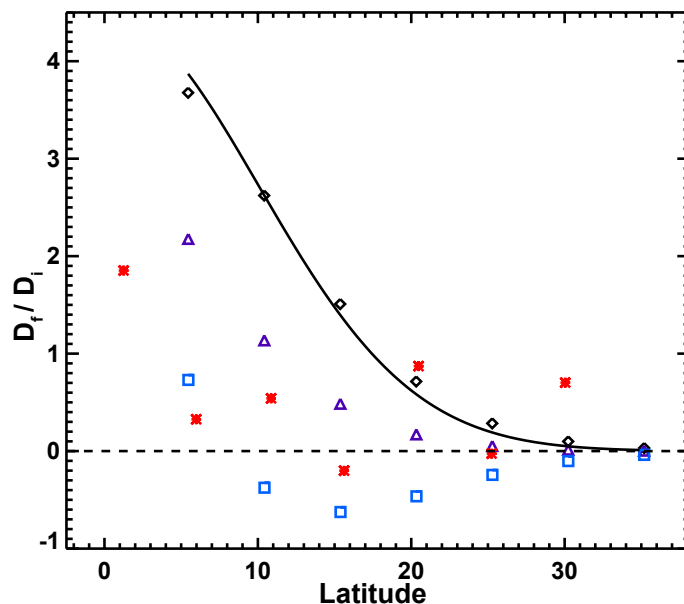


Fig. 4. Final dipole contribution factor D_f/D_i . The black diamonds represent the results of the symmetric bipolar ARs. The purple triangles represent the results of the weakly asymmetric bipolar ARs. The blue squares represent the results of the strongly asymmetric bipolar ARs. The red asterisks represent the results of the complex ARs. The black trend line representing Eq. (1) is fitted to the symmetric bipolar ARs. The black dashed horizontal line marks $D_f/D_i = 0$.

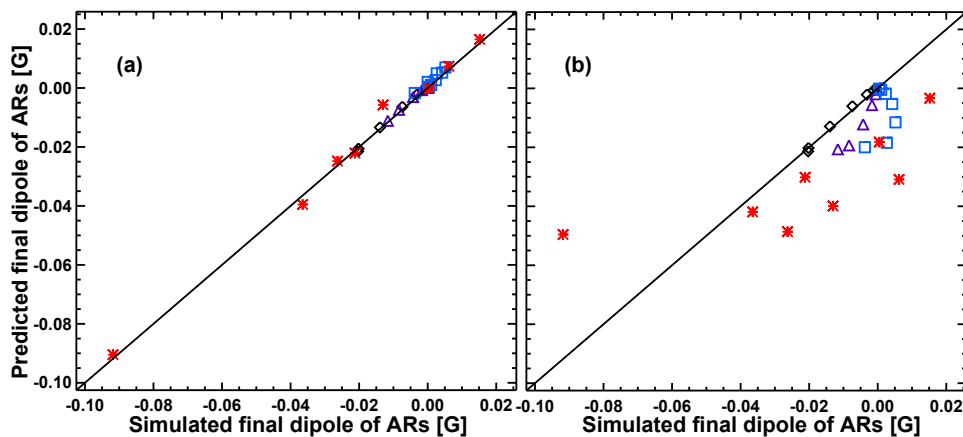


Fig. 5. Same as Figure 1, but for artificially created ARs. The black diamonds represent the results of the symmetric bipolar ARs. The purple triangles represent the results of the weakly asymmetric bipolar ARs. The blue squares represent the results of the strongly asymmetric bipolar ARs. The red asterisks represent the results of the complex ARs. Panel (a) presents the results of the generalized method that we introduce; panel (b) presents the results of the BMR-based method.

Schrijver (2001); Meyer & Mackay (2016); Upton & Hathaway (2018). These studies may reveal the effective range of the diffusion approximation for the magnetic flux evolution at the solar surface.

Acknowledgements. We thank the referee for the valuable comments and suggestions on improving the manuscript. The SDO/HMI data are courtesy of NASA and the SDO/HMI team. This research was supported by the Key Research Program of Frontier Sciences of CAS through grant No. ZDBS-LY-SLH013, National Natural Science Foundation of China through grant Nos. 11873023, 11322329, and 11533008, and the B-type Strategic Priority Program of CAS through grant No. XDB41000000. J.J. acknowledges the International Space Science Institute Teams 474 and 475.

References

- Babcock, H. W. 1961, *ApJ*, 133, 572
 Baumann, I., Schmitt, D., Schüssler, M., et al. 2004, *A&A*, 426, 1075
 Cameron, R. H., Dasi-Espuig, M., Jiang, J., et al. 2013, *A&A*, 557, A141. doi:10.1051/0004-6361/201321981
 Cameron, R. H., Jiang, J., Schmitt, D., et al. 2010, *ApJ*, 719, 264. doi:10.1088/0004-637X/719/1/264
 Cameron, R. H., & Schüssler, M. 2010, *ApJ*, 720, 1030
 Cameron, R. & Schüssler, M. 2015, *Science*, 347, 1333
 DeVore, C. R., Boris, J. P., Young, T. R., et al. 1985, *Australian Journal of Physics*, 38, 999
 Gizon, L. 2004, *Sol. Phys.*, 224, 217

- Hale, G. E., Ellerman, F., Nicholson, S. B., et al. 1919, *ApJ*, 49, 153
- Iijima, H., Hotta, H., & Imada, S. 2019, *ApJ*, 883, 24
- Jiang, J., Cameron, R., Schmitt, D., et al. 2010, *ApJ*, 709, 301
- Jiang, J., Cameron, R. H., Schmitt, D., et al. 2013, *A&A*, 553, A128. doi:10.1051/0004-6361/201321145
- Jiang, J., Cameron, R. H., & Schüssler, M. 2014, *ApJ*, 791, 5
- Jiang, J., Wang, J.-X., Jiao, Q.-R., et al. 2018, *ApJ*, 863, 159
- Jiang, J., Song, Q., Wang, J.-X., et al. 2019, *ApJ*, 871, 16
- Jiang, J. 2020, *ApJ*, 900, 19. doi:10.3847/1538-4357/abaa4b
- Leighton, R. B. 1964, *ApJ*, 140, 1547
- Leighton, R. B. 1969, *ApJ*, 156, 1
- Mackay, D. H., Priest, E. R., & Lockwood, M. 2002, *Sol. Phys.*, 209, 287
- Meyer, K. A. & Mackay, D. H. 2016, *ApJ*, 830, 160. doi:10.3847/0004-637X/830/2/160
- Mursula, K., Usoskin, I. G., & Maris, G. 2007, *Advances in Space Research*, 40, 885. doi:10.1016/j.asr.2007.07.046
- Nandy, D. & Martens, P. C. H. 2007, *Advances in Space Research*, 40, 891. doi:10.1016/j.asr.2007.01.079
- Nagy, M., Petrovay, K., Lemerle, A., et al. 2020, *Journal of Space Weather and Space Climate*, 10, 46. doi:10.1051/swsc/2020051
- Nagy, M., Lemerle, A., & Charbonneau, P. 2020, *Journal of Space Weather and Space Climate*, 10, 62. doi:10.1051/swsc/2020064
- Petrovay, K. 2020, *Living Reviews in Solar Physics*, 17, 2
- Petrovay, K., Nagy, M., & Yeates, A. R. 2020, *Journal of Space Weather and Space Climate*, 10, 50. doi:10.1051/swsc/2020050
- Schatten, K. H., Scherrer, P. H., Svalgaard, L., et al. 1978, *Geophys. Res. Lett.*, 5, 411. doi:10.1029/GL005i005p00411
- Schrijver, C. J. 2001, *ApJ*, 547, 475. doi:10.1086/318333
- Snodgrass, H. B. 1983, *ApJ*, 270, 288
- Upton, L. A. & Hathaway, D. H. 2018, *Geophys. Res. Lett.*, 45, 8091. doi:10.1029/2018GL078387
- van Ballegoijen, A. A., Cartledge, N. P., & Priest, E. R. 1998, *ApJ*, 501, 866
- Wang, Y.-M., Nash, A. G., & Sheeley, N. R. 1989, *ApJ*, 347, 529
- Wang, Y.-M. 2017, *Space Sci. Rev.*, 210, 351
- Wang, Z.-F., Jiang, J., Zhang, J., et al. 2020, *ApJ*, 904, 62. doi:10.3847/1538-4357/abbc1e
- Yeates, A. R. 2020, *Sol. Phys.*, 295, 119. doi:10.1007/s11207-020-01688-y